Tunable Thermal Conductivity of Ferroelectric P(VDF-TrFE) Nanofibers via Molecular Bond Modulation

Lan Dong(董岚)[1,2], Bohai Liu(刘博海)[3], Yuanyuan Wang(王元元)[1,2*], and Xiangfan Xu(徐象繁)[3*]

[1]*School of Energy and Materials, Shanghai Polytechnic University, Shanghai 201209, China*
[2]*Shanghai Engineering Research Center of Advanced Thermal Functional Materials, Shanghai Polytechnic University, Shanghai 201209, China*
[3]*Center for Phononics and Thermal Energy Science, China-EU Joint Center for Nanophononics, School of Physics Science and Engineering, Tongji University, Shanghai 200092, China*

(Received 27 September 2022; accepted manuscript online 4 November 2022)

Dipoles in ferroelectric copolymer P(VDF-TrFE) can be driven by electric field, introducing phonon transport modulations via polarizing molecular chains. The thermal conductivity in single 75/25 P(VDF-TrFE) nanofibers is found to increase with electric field related phonon renormalization, resulted from change in vibrational assignment excited by polarization process. This is evidenced by a direct change of bond energy and bond length in 75/25 P(VDF-TrFE) nanofibers from Raman characterization under polarization electric field. The experimental results provide further intuitive evidences that the size of ferroelectric polymers could directly affect the ferroelectricity from the size-dependent thermal transport measurement.

DOI: 10.1088/0256-307X/39/12/127201

The spontaneous electrical polarization of ferroelectrics is crucial to the semiconductor mechanism research and many of current applications that are related to tunable field-effect transistors[1,2] and non-volatile random access memories,[3–5] etc. Ferroelectrics usually have piezoelectric properties that generated tremendous interests in electrical field applications including energy storage, actuators, and sensors.[6–9] Rochelle salts[10] was discovered in the last century, whose polarization undergoes a hysteresis loop with electric field,[11–13] similar to the magnetic hysteresis loop in ferromagnetic materials.[14,15] Rochelle salts founded a new stage among numerous ferroelectric researches and also developed the field which has been dominated by inorganic ferroelectrics such as $Pb(Zr_xTi_{1-x})O_3$ (PZT)[16,17] and $BaTiO_3$.[18] Inorganic ferroelectrics have been exploited to develop the energy-efficient technology for micro-nano logic devices[19] as well as non-volatile random storages. However, essentially poisonous and preparation obstacles make applications of inorganic ferroelectrics severely restricted.

As polymer ferroelectrics, polyvinylidene fluoride (PVDF) and its copolymer poly(vinylidenefluoride-co-trifluoroethylene) [P(VDF-TrFE)] are both fluorine-based polymers, which are widely used in modern electronics and electrical systems due to their high dielectric constant and breakdown strength. Recent years, many researches focused on improving the energy density of the PVDF and its copolymer which could further optimize the breakdown strength and discharge efficiency in capacitive energy storage.[20,21] One key research topic is the physical properties and stability of polyvinylidene fluoride and its copolymer under extreme condition like ultra-high voltage with voltage gradient approaching breakdown threshold. In addition, heat dissipation is a critical issue that should be addressed immediately to improve long-term reliability and performances of electronics. PVDF and its copolymers need to pay attention to their heat dissipation properties while optimizing their electric performance. Therefore, the research on the thermal transport of PVDF and its copolymer P(VDF-TrFE) under high voltage becomes particularly important.[22] The regulation of polymer thermal transport is affected by micro/nano transport mechanisms, including hydrogen bond,[23] phonon coupling,[24] interface thermal transport,[25] etc. Therefore, the regulation mechanism of thermal transport in ferroelectric polymers needs to be more detailed.

Semi-crystalline ferroelectric PVDF and P(VDF-TrFE) hold spontaneous polarization based on its intrinsic structural polarization on both the sides of the C–C backbone.[26,27] In principle, there are four crystallize phases of fluorine-based ferroelectric polymers with different chain conformations, e.g., α-, β-, γ- and δ-phases.[28–33] The α-phase, the dominate phase in PVDF conformation, is non-polar with very weak ferroelectricity. Compared to weak ferroelectricity in α-phase, β-phase has an all-trans planar-zigzag chain conformation, which is highly polar structure. Among the four crystalline phases, α-phase is the non-polar phase but the most stable phase, therefore it is the most likely polymerization during the synthesis process of fluorine-based ferroelectric polymers. While for the β-phase (polar phase), the requirements for polymerization of fluorine-based polymers are more stringent and complex because of the instability of β-phase. P(VDF-TrFE) is a typical PVDF copolymer with excellent ferroelectric properties, with its chain conformation mainly composed of β-phase. TrFE is the key point for the formation of β-phase, the higher mole fraction of TrFE can achieve the better ferroelectricity of P(VDF-TrFE).[34]

*Corresponding authors. Email: wangyuanyuan@sspu.edu.cn; xuxiangfan@tongji.edu.cn
© 2022 Chinese Physical Society and IOP Publishing Ltd

It is the inherent property of ferroelectric system that the dipole can be driven by an applied polarization electric field. The polymer ferroelectrics have intrinsic dipoles whose polarization direction is perpendicular to the C–C backbones. The electrostatic force generated by the applied electric field is believed to affect the bond length, bond angle and the atomic vibration modes in ferroelectric systems. However, the change of chain configuration is not easy to be observed in bulk ferroelectric polymers due to the complicated and confused molecular chain structures of polymers. In order to explore the coupling relationship between chain configuration and applied polarization electric field, P(VDF-TrFE) nanofibers are prepared *in situ* on micro-electro-mechanical system (MEMS) devices using electrospinning process, suitable for thermal transport measurement. The electrospinning process forces the molecular chain align along the longitudinal direction of nanofibers. Such a structural optimization is helpful for further studying the change of the bond length, bond angle and the atomic vibration modes in ferroelectric polymers, which is believed to affect the thermal properties of the ferroelectric nanofiber, however has not yet been studied experimentally so far.

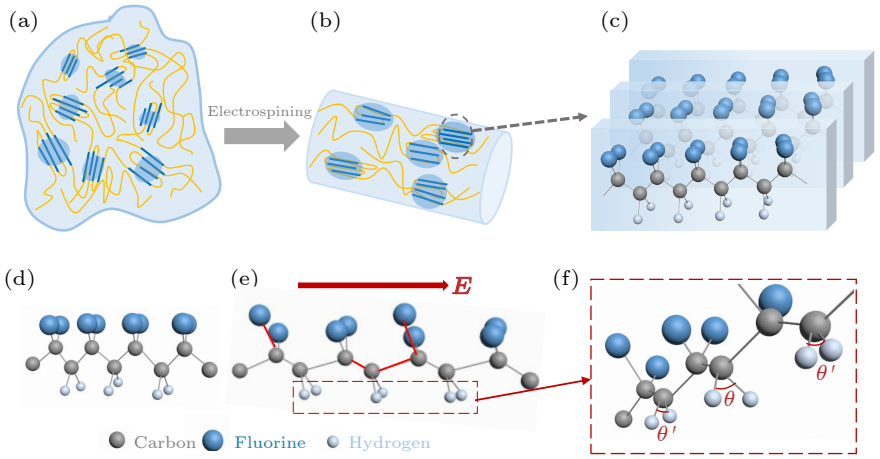

Fig. 1. Schematic of molecular conformation under polarization electric field and the morphology details of ferroelectric P(VDF-TrFE). (a) Isotropic bulk P(VDF-TrFE) system with the chain ends, entanglements, voids and defects. (b) Schematic of molecular chain orientation of P(VDF-TrFE) nanofiber after electrospinning process with no polarization electric field applied. The light blue circle areas represent the crystalline regions, the yellow lines represent the amorphous regions. (c) The arrangement of β-phase in crystalline regions of P(VDF-TrFE) nanofiber. (d) The molecular chains of typical β-phase of P(VDF-TrFE) under zero field. (e) The change of bond energy, bond length and bond angle of β-phase chains under polarization electric field (red arrow). The red lines represent the change of bond length of C–C bond and CF_2 bond, the red dashed rectangle represents the change of angles of CH_2 bonds. (f) Enlarged image exhibits the changed angles of CH_2 bonds.

The bulk semi-crystalline polymers contain both aligned crystalline and chain-oriented amorphous phases, with the crystalline region surrounded by the random amorphous regions.[35] Bulk P(VDF-TrFE) contains the chain ends, entanglements, voids and defects that inhibit the inter and intra molecular thermal transport [shown in Fig. 1(a)], resulting in inferior thermal conductivity (0.1–0.3 $W{\cdot}m^{-1}{\cdot}K^{-1}$) compared to that in aligned molecular chains and nanofibers.[36,37] Electrospinning is a mature and widely used technology for polymer nanofiber preparation, with its electric voltage generally ranging from thousands of volts to tens of thousands of volts. Under the electrostatic force created by the high voltage, the polymer solution is first stretched into an ellipsoid, and then nanofibers with diameters in the order of micrometers or nanometers are prepared at the front end of the ellipsoid. The polymer nanofiber prepared by electrospinning technique could help align the molecular chains (anisotropic nanofibers) and decrease the phonon scattering which is the main factor restricting the thermal conductivity of polymers [shown in Fig. 1(b)]. Crystalline phase in semi-crystalline polymers appears as the folded chain regions. For copolymer P(VDF-TrFE), it has well-arranged H-F dipoles, whose polarization direction is perpendicular to the C–C backbone [details could be found in Fig. 1(c)]. In this experiment, single P(VDF-TrFE) nanofibers [the molar ration of P(VDF-TrFE) is 75/25, which was purchased from PIEZOTECH company] are prepared across the two thermometers of the MEMS device. Considering the anisotropy of molecular chain orientation caused by electrospinning process, an applied polarization electric field E was provided parallel to the orientation direction of the C–C backbones, which is also the axial direction of the P(VDF-TrFE) nanofibers. Figure 1(d) exhibits the β-phase molecular chains of P(VDF-TrFE) without polarization electric field ($E = 0$), whose dipole direction is perpendicular to the arrangement direction of the C–C chain. The bond length of C–C band and side chains will change to some extent [represented by the red lines in Fig. 1(e)] under polarization electric field. The variation of bond length is consistent with assumptions in the previous work.[38]

The changes of bond energy, bond length and bond angle are the direct factors affecting the thermal transport of nanostructures, especially in polymer nanofibers. In order to observe the change of thermal conductivity

caused by the polarization electric field mentioned above, thermal bridge method was used to characterize the axial thermal conductivity of P(VDF-TrFE) nanofibers with molar ratio 75/25. The whole suspended MEMS device was placed in a cryostat with high vacuum on the order of 1×10^{-5} Pa to reduce the effect of thermal convection. Considering the change in thermal conductivity of a single P(VDF-TrFE) nanofiber would be much lower than the measurement sensitivity of traditional thermal bridge method,[39–43] we adopted the differential circuit configuration due to its advanced measurement sensitivity approaching to ~ 10 pW/K.[44]

Figure 2(a) is the SEM image of a suspended single P(VDF-TrFE) nanofiber with 75/25 molar ratio (sample 1: 75/25). The nanofiber was fabricated across the two Pt/SiN_x thermometers by electrospinning technology.[45] After electrospinning the P(VDF-TrFE) nanofiber needs to be annealed at 140 ℃ in high purity nitrogen environment to improve its crystallization of β-phase.[46] The red arrow illustrates the direction of the polarization electric field. It is the key step where the tunable molecular conformation gradually affects the phonons transport along the axis of the P(VDF-TrFE) nanofiber. To avoid the interaction between pluralities of nanofibers, we prepared a single suspended nanofiber that is extremely difficult for electrospinning to measure the polarization tunable thermal conductivity. Figure 2(b) presents the enlarged nanofiber morphology of sample 1 with molar ratio 75/25. The morphology details of the single P(VDF-TrFE) electrospinning nanofibers with 75/25 molar rations in this experiment are illustrated in Table 1. In order to ensure the reliability of our experimental results, we prepared two 75/25 P(VDF-TrFE) nanofibers with different diameters and characterize their polarization tunable thermal conductivities separately.

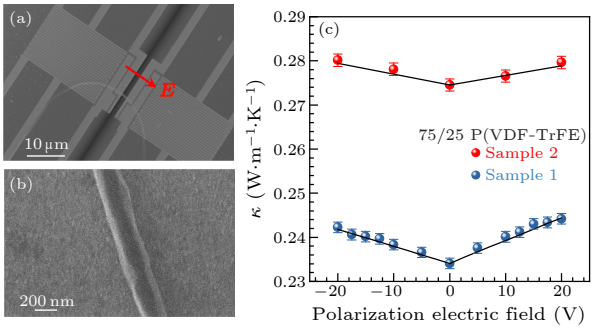

Fig. 2. Polarization tunable thermal transport of P(VDF-TrFE) nanofibers with 75/25 molar ratio at $T = 300$ K. (a) SEM image of a single 75/25 P(VDF-TrFE) nanofiber suspended on the MEMS device for thermal transport measurement, with the scale bar being 10 μm. The middle electrodes of MEMS device are used to add the polarization electric field. The polarization electric field is provided by the Keithley 6430 and the red arrow indicates its direction. (b) Enlarged SEM image of the same P(VDF-TrFE) nanofibers in (a). The scale bar is 200 nm. (c) Thermal conductivities of nanofibers 1 and 2 with the change of polarization electric field. As the positive electric field approaches to 20 V, the thermal conductivity of sample 1 increases by 4.3% compared with the unpolarized thermal conductivity, while for negative electric field (up to −20 V) the increase of thermal conductivity reaches 3.5%. Thermal conductivity increases by 1.9% with the highest positive electric field (+20 V) and 2.0% with the highest negative electric field (−20 V) for sample 2. The black solid lines are fitted by formula (1).

Table 1. The diameters, thermal conductivities and ϕ results of phonon renormalization of P(VDF-TrFE) nanofibers with different molar ratios.

	Diameter (nm)	κ_0 (W·m^{-1}·K^{-1})	Positive field ϕ	Negative field ϕ
Sample 1, 75/25	178	0.23	3.35 ± 0.3	4.4 ± 0.4
Sample 2, 75/25	158	0.27	1.6 ± 0.15	1.8 ± 0.2
Sample 3,[38] 70/30	138	1.52	3.7 ± 0.5	3.7 ± 0.4
Sample 4,[38] 70/30	511	1.10	7.9 ± 0.6	5.5 ± 0.7

The thermal conductivity of 75/25 P(VDF-TrFE) nanofibers was measured as the polarization electric field increased. Here we focused on the mechanism of thermal transport induced by the polarization electric field. As shown in Fig. 2(c), when the polarization electric field reaches ±20 V, the thermal conductivity of the two samples exhibit the different increments. The thermal conductivity of nanofiber 1 approaches to 0.23 W·m^{-1}·K^{-1} under the zero field, which increases by 4.3% for 20 V and 3.5% for −20 V. Consistent experimental conditions are provided for the thermal conductivity measurement of nanofiber 2 and we found that the zero field thermal conductivity is 0.27 W·m^{-1}·K^{-1}. For nanofiber 2, the increments of thermal conductivity approach to 1.9% and 2.0% for 20 V and −20 V polarization voltages. The differences under positive and negative polarized electric fields are obviously observed, which are believed due to the inherent hysteresis property of ferroelectric materials. In our experiments, the highest electric potential gradient is 20 MV/m, which is much lower than the coercive electric field of P(VDF-TrFE) ~ 55 MV/m. Similar enhancement of thermal conductivity in P(VDF-TrFE) film has been observed in the work of Deng *et al.*, and the thermal conductivity under 80 MV/m potential gradient presented 53% higher than film.[47] Compared with previous inorganic crystalline $Pb(Zr_{0.3}Ti_{0.7})O_3$ film,[48] the increment of thermal conductivity is 0.23% per MV/m under polarization voltage, which is similar with the increment ($\sim 0.22\%$ per MV/m) in our P(VDF-TrFE) nanofiber. Our P(VDF-TrFE) amorphous nanofibers could obtain such a prominent increment in thermal conductivity under the polarized electric field like crystalline ferroelectrics. We believe that this increment in P(VDF-TrFE) nanofibers may be influenced by the phonon renormalization, which will be discussed later.

In addition, we found that the thermal conductivities of nanofibers with 70/30 molar ratio present much higher values than those of 75/25 molar ratio nanofibers whose

values are still in the range of bulk polymers, i.e., $\sim$0.1–0.3 $W{\cdot}m^{-1}{\cdot}K^{-1}$. P(VDF-TrFE) with 70/30 molar ration has the higher mole fraction of TrFE and is generally considered to have better ferroelectric properties (see Table 1). It is possible that there is thermal percolation in the P(VDF-TrFE) nanofiber with 70/30 molar ratio, which needs to be further verified by more experiments in the future.[49]

We now turn to understand the physics behind the electric-field-dependent thermal conductivity. Phonon renormalization is believed to be responsible for the measured thermal conductivity. According to the phonon renormalization, the molecules of the ferroelectric polymers will deviate from the equilibrium position under the polarization, and the change of bond length and bond energy become the main factors affecting the phonon transport in P(VDF-TrFE) nanostructures. Based on the phonon renormalization model, the thermal conductivity of ferroelectric polymer under polarization electric field can be expressed as[38]

$$\kappa = \kappa_0\sqrt{1+\phi E}, \tag{1}$$

where κ_0 is the thermal conductivity of 75/25 P(VDF-TrFE) nanofibers under zero field. E is the polarization electric field (the absolute value should be used to calculate the thermal conductivity), and ϕ is related to the ferroelectricity of nanofiber. The higher ϕ indicates better ferroelectricity.

We compared the ϕ results of previous P(VDF-TrFE) nanofibers with 70/30 molar ratio (shown in Table 1). There are two importance observations: (1) It can be concluded that the 75/25 P(VDF-TrFE) with smaller ϕ has poor ferroelectricity, which is consistent with the previous results.[50,51] (2) Nanofibers with larger diameter hold the higher ϕ for both positive and negative electric fields. The larger diameter of ferroelectric polymer nanofiber contains more polar phase (β-phase), and the effect of phonon renormalization of molecular chains becomes more obvious.

Polarization electric field should affect bond length, bond energy, and bond angle. In the phonon renormalization model, the change of band angle is not taken into account. However, it is undeniable that the thermal conductivity of the P(VDF-TrFE) nanofiber would be affected by change of the bond angle.[52]

Table 2. Vibrational assignment of P(VDF-TrFE) in the range 650–1600 cm^{-1}. The uncertainty of the vibrational frequencies is obtained from the Gauss fit results.

β-phase P(VDF-TrFE)				
Vibrational assignment[53]	Theory[32] $E = 0$ V (cm^{-1})	Experiment[54] $E = 0$ V (cm^{-1})	This work $E = 0$ V (cm^{-1})	This work $E = 20$ V (cm^{-1})
CF_2 stretch	840	845	836 ± 0.42	842 ± 0.80
CH_2 scissoring & CF_2 stretch	1281	1289		1292
C–C stretch & CH_2 wag	1409	1402	1400 ± 0.17	1397 ± 0.26
C–C stretch & CH_2 scissoring	1442	1431	1429 ± 0.30	1431 ± 0.12

In order to confirm the prediction of bond length and bond energy in phonon renormalization model, here the Raman spectra were characterized to determine the change of molecular bonds under polarization electric field. Raman spectroscopy is one of the most common methods to characterize molecular bond energy, bond vibration and bond rotation.[53,54] For fluorine-based ferroelectric polymers [PVDF and P(VDF-TrFE)], non-polar phase (α-phase) and polar phase (β-phase) could be directly resolved from Raman feature bonds according to the previous results.[54] In order to clarify the variation of bond length of P(VDF-TrFE) under the polarization electric field E, Raman responses were studied with 20 V electric field and 0 V electric field, respectively (shown in Fig. 3 and Table 2). The shifts of Raman peaks can clearly reflect the changes of bond length and bond energy of P(VDF-TrFE) molecular chains. It is no dispute that the electric field only affects the polar phase, thus we should only focus on the change of β-phase in the experimental results. To realize the added polarization field between the two ends of the nanofiber, we choose two middle electrodes of the MEMS device to apply voltage, as indicated in Fig. 2(a).

Figure 3 presents the Raman spectra of a single 75/25 P(VDF-TrFE) nanofiber under different polarization electric fields (0 V and 20 V). Figure 3(a) shows the Raman transition of the 75/25 P(VDF-TrFE) nanofiber in the range 650–1600 cm^{-1}, which is located in the region of β-phase. Figure 3(b) is the enlarged Raman spectra in the range from 825 cm^{-1} to 852 cm^{-1}. We can find an obvious peak with wavenumber at 836 cm^{-1} under 0 V (represented by blue line). The peak at 840 cm^{-1} is the same typical characteristic of β-phase in theoretical calculation, which represents the CF_2 stretch vibration (shown in Table 2).[54,55] After adding the polarization electric field ($E = 20$ V), the 836 cm^{-1} peak exhibits a significant blue shift to 842 cm^{-1} (represented by orange line). This blue shift reflects that the bond energy of CF_2 bond appears increasing trend. The enhancement of CF_2 bond energy is due to the bond length stretched by polarization electric field, which directly increases the bond energy of CF_2 bond under stress. The bond length stretched by polarization electric fields could also be found in previous work. Mollica *et al.*[56] testified the atomic displacement (C–C and C–N bonds) caused by the oriented external electric field in the indigo molecule. Bystrov *et al.*[57] also gave clear evidence for the change of bond length under electric field in the PVDF system.

The change of CF_2 bond length is shown in the schematic diagram of Fig. 3(b). Figure 3(c) presents the change of carbon–carbon molecular bonds. In theory, 1409 cm^{-1} is a characteristic peak of C–C stretch and CH_2 wag vibration, and 1442 cm^{-1} peak presents the C–C

stretch and CH_2 scissoring vibration. Neither CH_2 wag nor CH_2 scissoring will change the bond length, thus these vibrations do not produce peak shift. In our experiments we find the corresponding peaks at 1400 cm^{-1} and 1429 cm^{-1} under 0 V field. After adding electric field, the 1400 cm^{-1} peak appears red shift to 1397 cm^{-1} that exhibits the decreasing bond energy only in C–C bond and the 1429 cm^{-1} peak shows blue shift to 1431 cm^{-1} that presents the increasing C–C bond energy. The changes of wavenumbers of 1400 cm^{-1} peak and 1429 cm^{-1} peak expound that the carbon atom will deviate from the equilibrium position under the effect of polarization electric field corresponding to the phonon renormalization model, and the bond length of the adjacent C–C bond will increase and decrease at the same time [shown in Fig. 3(c)]. In addition, we also found a Raman peak around 1292 cm^{-1} that can characterize the change of CH_2 bond angle after adding electric field.

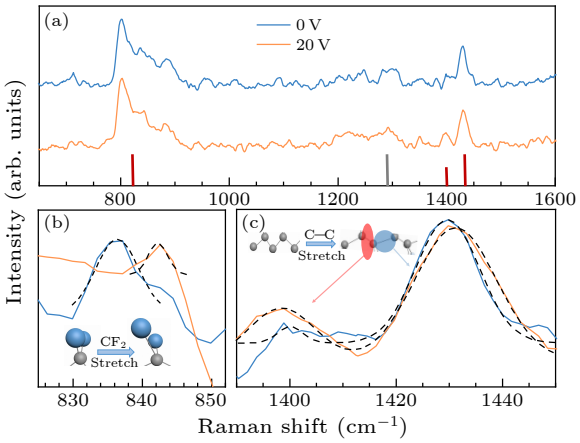

Fig. 3. Raman spectra of the suspended single P(VDF-TrFE) nanofiber with 75/25 molar ratio. The blue lines represent the Raman spectra under 0 V, and the orange lines under 20 V. (a) Raman spectra of the P(VDF-TrFE) nanofiber with Raman shift in the range from 650 cm^{-1} to 1600 cm^{-1}. (b) Enlarged wavenumbers ranging from 825 cm^{-1} to 852 cm^{-1}, among which the peak of CF_2 bond is observed. The result illustrates an obvious blue shift under polarization electric field and indicates the bond length increase of CF_2 bond. (c) Raman spectra in the range of C–C bond. After applying the polarization electric field, the peak near 1400 cm^{-1} exhibits the red shift, representing that the C–C bond length becomes shorter, while the peak near 1429 cm^{-1} appears blue shift, representing that the C–C bond length becomes longer. The dotted dark lines are peak position fitting.

The peak shift of C–C bond confirms that the phonon renormalization appears in the P(VDF-TrFE) nanofiber. The applied polarization electric field leads to a red shift of the peak near 1400 cm^{-1} and a blue shift near 1429 cm^{-1} of C–C bond, which has been intuitively shown in the inserted schematic diagram in Fig. 3(c). From the schematic diagram, we find that adjacent C–C bonds in the P(VDF-TrFE) backbone cannot be longer or shorter at the same time under the strength of the polarization electric field. The C–C bond becomes shorter in red circle and becomes longer in blue circle. This difference of C–C length may be explained such that the carbon atoms will be displaced from the original equilibrium positions in the process of phonon renormalization (caused by applied polarization electric field) and the adjacent carbon atoms will move in the opposite direction. The harmonic approximation of the potential at the new equilibrium position will be different from the original one due to the anharmonicity. Therefore, the lattice constant and bond energy are different from those in unpolarized molecular bonds.

In conclusion, the polarization electric field could induce the changes of bond energy, bond length and bond angle of the ferroelectric polymers. The changes of bond length and bond energy are the key points of the increasing thermal conductivities of the P(VDF-TrFE) nanofibers, evidenced from the Raman spectra which directly prove the polarization induced phonon renormalization of fluorine-based polymers. In addition, the 75/25 P(VDF-TrFE) nanofiber contains inferior ferroelectricity compared to the 70/30 P(VDF-TrFE) nanofiber and the large diameter nanofiber will have more polar phases and better ferroelectricity.

Methods. Firstly, we describe the preparation of the suspended MEMS device. The supported MEMS device was processed by previous micro-nano procedures, including ultraviolet lithography, metal deposition (Pt electrodes deposited on the SiN_x beam), lift-off and deep reactive ion etching. After potassium hydroxide (KOH solution 30 vol%) wet etching, the suspended MEMS devices were fabricated before electrospinning process. The KOH solution was mainly used for etching the silicon oxide substrate which is not covered by Pt/SiN_x electrodes. In order to prevent the suspended Pt/SiN_x electrodes from being broken by the tension of the solution (KOH solution, deionized water, etc.), in our experiments we used a critical dryer (Tousimis Samdri-PVT-3D) to dry the MEMS device and to protect the suspended electrodes. After KOH wet etching, the whole suspended MEMS devices are annealed in H_2/Ar atmosphere at around 250 ℃ for 2–3 h to remove the water molecules and polymer residues on the surface of the device. Electrospinning process was carried out immediately after H_2/Ar atmosphere annealing to prevent the accumulation of water molecules on the electrode from affecting the thermal contact between the P(VDF-TrFE) nanofiber and the Pt/SiN_x electrodes.

Secondly, we present the electrospinning. The electrospinning solvent, a mixture of P(VDF-TrFE) powder and dimethylformamide (DMF) solution, was prepared with 12 wt% to 18 wt%. Usually, P(VDF-TrFE) solution should be stirred at room temperature for more than 12 h to ensure the complete dissolution of P(VDF-TrFE) powder. Considering that we needed to apply a large enough potential gradient to both ends of the P(VDF-TrFE) nanofiber, here we chose the suspended MEMS device with a gap no more than 3 μm between the two thermometers to fabricate the suspended P(VDF-TrFE) nanofibers. We fixed the syringe speed (0.5 mL/h) and the distance (20 cm) between the needle tip and the MEMS device during the electrospinning process, and we found that the diameter of P(VDF-TrFE) nanofibers is related to the high voltage (9–13 kV) and solution concentration. To fabricate a suspended single P(VDF-TrFE) nanofiber across the two thermometers and the electrodes which were used to add the polarization electric field, the electrospinning time is

controlled within 10 s.

Thirdly, we introduce the thermal bridge method. The thermal conductivity of a suspended single P(VDF-TrFE) nanofiber can be characterized by the thermal bridge method. In order to reduce the effect of thermal convection, the whole suspended MEMS device with a single P(VDF-TrFE) nanofiber was placed into a cryostat with high vacuum on the order of 1×10^{-4} Pa. We waited for at least two hours at each temperature point to ensure the stability of the ambient temperature. To provide heating power, a 10 μA DC current (provided by Keithley 6221) is added to the one thermometer severed as heater to produce the total joule heat. After reaching thermal equilibrium, the same AC currents (~ 1 μA provide by Keithley 6221) were used to observe the change of resistance of the two thermometers which acted as the above-mentioned heater and sensor. The changes of voltages on the heater and sensor were measured by a lock-in amplifier (SRS 830). The change of resistance of thermometers could characterize the temperature rises ($\Delta T_{\rm h}$ and $\Delta T_{\rm s}$) of both the ends of the P(VDF-TrFE) nanofiber. Here the thermal conductance of the P(VDF-TrFE) nanofiber ($G_{\rm P(VDF\text{-}TrFE)}$) could be calculated by the thermal equilibrium formula:

$$G_{\rm b} = \frac{Q_{\rm tot}}{\Delta T_{\rm h} + \Delta T_{\rm s}},$$
$$G_{\rm P(VDF\text{-}TrFE)} = \frac{G_{\rm b}\Delta T_{\rm s}}{\Delta T_{\rm h} - \Delta T_{\rm s}},$$

where $Q_{\rm tot}$ is total joule heat added on the heater, $G_{\rm b}$ is the thermal conductance of the Pt/SiN_x beams, $\Delta T_{\rm h}$ and $\Delta T_{\rm s}$ act as the temperature rises of the heater and sensor, respectively. The thermal conductivity of a single P(VDF-TrFE) nanofiber could be obtained by

$$\kappa = G_{\rm P(VDF\text{-}TrFE)}\frac{L}{A}.$$

Here, κ is the thermal conductivity of the P(VDF-TrFE) nanofiber, L and A are the length and cross section of the P(VDF-TrFE) nanofiber.

Acknowledgement. This work was supported by the National Natural Science Foundation of China (Grant Nos. 12004242, 11890703, 12174286, 11935010, and 51876111), the Key-Area Research and Development Program of Guangdong Province (Grant No. 2020B010190004), the Shanghai Rising-Star Program (Grant No. 21QA1403300), and the Shanghai Local Capacity Building Program (Grant No. 22010500700).

References

[1] Zheng Y, Ni G X, Toh C T, Tan C Y, Yao K, and Ozyilmaz B 2010 *Phys. Rev. Lett.* **105** 166602
[2] Sun Y L, Xie D, Xu J L, Li X M, Li X, Zhang C, Dai R X, Meng X J, and Zhu H W 2016 *Carbon* **96** 695
[3] Scott J F and de Paz A C A 1989 *Science* **246** 1400
[4] Lipatov A, Sharma P, Gruverman A, and Sinitskii A 2015 *ACS Nano* **9** 8089
[5] Boyn S, Girod S, Garcia V, Fusil S, Xavier S, Deranlot C, Yamada H, Carretero C, Jacquet E, Bibes M, Barthelemy A, and Grollier J 2014 *Appl. Phys. Lett.* **104** 52909
[6] Kim J, Lee J H, Ryu H, Lee J H, Khan U, Kim H, Kwak S S, and Kim S W 2017 *Adv. Funct. Mater.* **27** 1700702
[7] Chang J Y, Dommer M, Chang C, and Lin L W 2012 *Nano Energy* **1** 356
[8] Crossley S, Whiter R A, and Kar-Narayan S 2014 *Mater. Sci. Technol.* **30** 1613
[9] Kaczmarek H, Królikowski B, Klimiec E, Chylińska M, and Bajer D 2019 *Russ. Chem. Rev.* **88** 749
[10] Lim A R and Lee K S 2011 *J. Appl. Phys.* **110** 033520
[11] Tayi A S, Kaeser A, Matsumoto M, Aida T, and Stupp S I 2015 *Nat. Chem.* **7** 281
[12] Abolhasani M M, Zarejousheghani F, Cheng Z, and Naebe M 2015 *RSC Adv.* **5** 22471
[13] Wang X L, Li B, Zhong X L, Zhang Y, Wang J B, and Zhou Y C 2012 *J. Appl. Phys.* **112** 114103
[14] Singha A, Donati F, Wäckerlin C, Baltic R, Dreiser J, Pivetta M, Rusponi S, and Brune H 2016 *Nano Lett.* **16** 3475
[15] Goodwin C A P, Ortu F, Reta D, Chilton N F, and Mills D P 2017 *Nature* **548** 439
[16] Kushida-Abdelghafar K, Miki H, Torii K, and Fujisaki Y 1996 *Appl. Phys. Lett.* **69** 3188
[17] Lee W, Kahya O, Toh C T, Ozyilmaz B, and Ahn J H 2013 *Nanotechnology* **24** 475202
[18] Xiong C, Pernice W H P, Ngai J H, Reiner J W, Kumah D, Walker F J, Ahn C H, and Tang H X 2014 *Nano Lett.* **14** 1419
[19] Yu H, Chung C C, Shewmon N, Ho S, Carpenter J H, Larrabee R, Sun T, Jones J L, Ade H, O'Connor B T, and So F 2017 *Adv. Funct. Mater.* **27** 1700461
[20] Guo M F, Jiang J Y, Shen Z H, Lin Y H, Nan C W, and Shen Y 2019 *Mater. Today* **29** 49
[21] Dang Z M, Yuan J K, Yao S H, and Liao R J 2013 *Adv. Mater.* **25** 6334
[22] Li Z, Zhang L, Qi R, Xie F, and Qi S 2016 *RSC Adv.* **6** 35884
[23] Deng S, Ma D, Zhang G, and Yang N 2021 *J. Mater. Chem. A* **9** 24472
[24] Pan D K, Zong Z C, and Yang N 2022 *Acta Phys. Sin.* **71** 086302 (in Chinese)
[25] An M, Sun X H, Chen D S, and Yang N 2022 *Acta Phys. Sin.* **71** 166501 (in Chinese)
[26] Mahdi R I, Gan W C, Abd M W H, Mukri N I, and Furukawa T 2018 *Polymer* **141** 184
[27] da Silva A B, Wisniewski C, Esteves J V A, and Gregorio R 2010 *J. Mater. Sci.* **45** 4206
[28] Hasegawa R, Takahashi Y, Chatani Y, and Tadokoro H 1972 *Polym. J.* **3** 600
[29] Hasegawa R, Kobayashi M, and Tadokoro H 1972 *Polym. J.* **3** 591
[30] Bachmann M, Gordon W, Weinhold S, and Lando J 1980 *J. Appl. Phys.* **51** 5095
[31] Li M Y, Wondergem H J, Spijkman M J, Asadi K, Katsouras I, Blom P W M, and De Leeuw D M 2013 *Nat. Mater.* **12** 433
[32] Milani A, Castiglioni C, and Radice S 2015 *J. Phys. Chem. B* **119** 4888
[33] Takahashi Y, Matsubara Y, and Tadokoro H 1983 *Macromolecules* **16** 1588
[34] Lovinger A J, Davis G T, Furukawa T, and Broadhurst M 1982 *Macromolecules* **15** 323
[35] Xi Q, He J, Xu X, Nakayama T, Wang Y, Liu J Z J, and Li B 2020 *Chin. Phys. Lett.* **37** 104401
[36] Henry A and Chen G 2008 *Phys. Rev. Lett.* **101** 235502
[37] Liu J and Yang R 2012 *Phys. Rev. B* **86** 104307
[38] Dong L, Xi Q, Zhou J, Xu X, and Li B 2020 *Phys. Rev. Appl.* **13** 034019
[39] Xu X F, Pereira L F C, Wang Y, Wu J, Zhang K W, Zhao X M, Bae S, Tinh B C, Xie R G, Thong J T L, Hong B H, Loh K P, Donadio D, Li B W, and Özyilmaz B 2014 *Nat. Commun.* **5** 3689

[40] Guo J, Huang Y, Wu X, Wang Q, Zhou X, Xu X, and Li B 2019 *Phys. Status Solidi RRL* **13** 1800529

[41] Aiyiti A, Zhang Z, Chen J, Chen B, Hu S, Xu X, and Li B 2018 *Carbon* **140** 673

[42] Xu X, Zhou J, and Chen J 2020 *Adv. Funct. Mater.* **30** 1904704

[43] Dong L, Xu X, and Li B 2018 *Appl. Phys. Lett.* **112** 221904

[44] Dong L, Xi Q, Chen D S, Guo J, Nakayama T, Li Y, Liang Z, Zhou J, Xu X, and Li B 2018 *Natl. Sci. Rev.* **5** 500

[45] Na H N, Chen P, Wong S C, Hague S, and Li Q 2012 *Polymer* **53** 2736

[46] Furukawa T, Nakajima T, and Takahashi Y 2006 *IEEE Trans. Dielect. Electr. Insul.* **13** 1120

[47] Deng S, Yuan J, Lin Y, Yu X, Ma D, Huang Y, Ji R, Zhang G, and Yang N 2021 *Nano Energy* **82** 105749

[48] Ihlefeld J F, Foley B M, Scrymgeour D A, Michael J R, McKenzie B B, Medlin D L, Wallace M, Trolier-McKinstry S, and Hopkins P E 2015 *Nano Lett.* **15** 1791

[49] Zhou J, Xi Q, He J, Xu X, Nakayama T, Wang Y, and Liu J 2020 *Phys. Rev. Mater.* **4** 015601

[50] Lu Y, He C, Song G, Wu B, Chung C H, and Lee Y C 2014 *Ultrasonics* **54** 296

[51] Guimarães N J M, Oliveira J O N, and Faria R M 2000 *Appl. Phys. A* **71** 267

[52] Zhang T, Wu X, and Luo T 2014 *J. Phys. Chem. C* **118** 21148

[53] Cortili G and Zerbi G 1967 *Spectrochim. Acta A* **23** 285

[54] Arrigoni A, Brambilla L, Bertarelli C, Serra G, Tommasini M, and Castiglioni C 2020 *RSC Adv.* **10** 37779

[55] Green J S, Rabe J P, and Rabolt J F 1986 *Macromolecules* **19** 1725

[56] Mollica N V, Cassone G, Ponterio R C, Saija F, Sponer J, Tommasini M, and Trusso S 2020 *J. Phys. Chem. A* **124** 10856

[57] Bystrov V S, Paramonova E V, Bdikin I K, Bystrova A V, Pullar R C, Kholkin A L 2013 *J. Mol. Model.* **19** 3591